Temporal changes of medium properties during explosive volcanic eruption

Supplementary Materials

Redoubt volcano and eruptions

Redoubt volcano is located in the northeastern Aleutian volcanic arc in the Cook Inlet, ∼170 km southwest from Anchorage, Alaska. The volcano is a glaciated stratovolcano fed by rhyolitic andesitic magma (Morrissey, 1997). Other active volcanoes (e.g., Augustine and Spurr) are located near Redoubt volcano. Redoubt volcano is 3108 m in height, 10-12 km in diameter at the base, and ∼1.5 km in diameter at the crater (Schaefer et al., 2009; Bull et al., 2013). The crater is filled with glaciers, breaching to the north. The Drift glacier stretches 5 km down to the Drift River Valley. The volcano erupted in 1902, 1933, 1966-1968, 1989-1990, and most recently in 2009 (Coombs et al., 2013).

The volcanic eruption of 1966-1968 generated pyroclastic flows that melted ∼60 Mm^3 (∼6 % of the total volume) of the Drift glacier. The melted glacier flows produced lahars (ash-mud flows), inundating the Drift River Valley. The lahars reached the mouth of the Drift River on the coast (Buurman et al., 2013). Redoubt volcano reerupted in mid-December 1989. It erupted 25 times over four months in 1989-1990. These volcanic eruptions removed a significant volume of glacier, and built up sediments in the river by lahars. The 1989-1990 volcanic activity created 14 lava domes.

In May 2008, magma reascended from a depth of 25-38 km (lower crust) to a depth of 7-11.5 km (upper crust), forming a magma chamber and melting nearby rocks (Grapenthin et al., 2013). The magma ascent produced precursory signatures of eruption, such as heat flow increase and summit inflation with glacier melting (Bleick et al., 2013; Bull and Buurman, 2013; Grapenthin et al., 2013; Power et al., 2013). Magma ascended to a depth of 2-4.5 km below the volcano in Jan to Feb 2009, and the volcano eventually erupted in March 2009

Table 1. Numbers of events and data by eruption phase.

ID	phase (yyyy/mm/dd)	period	number of events	number of data
I	precursory	2009/01/01 - 2009/03/14	560	897
II	explosive	2009/03/15 - 2009/04/04	317	454
III	effusive	2009/04/05 - 2009/07/01	680	1635
IV	post-eruption	2009/07/02 - 2009/12/31	162	414
V	post-eruption	2010/01/01 - 2010/12/31	219	443
total		2009/01/01 - 2010/12/31	1936	3843

(Coombs et al., 2012; Power et al., 2013). The volume of magma in the upper crust decreased during eruption (Grapenthin et al., 2013).

The 2009 eruption period can be divided into four phases: precursory, explosive, effusive, and post-eruption phases (Schaefer, 2012; Bull and Buurman, 2013; Grapenthin et al., 2013; Table 1). The precursory phase lasted from July 2008 to 15 March 2009, the explosive phase from 15 March 2009 to 04 April 2009, and the effusive phase (lava-dome growth phase) from 4 April 2009 to July 2009 (Bull and Buurman, 2013; Grapenthin et al., 2013). The volcano was stabilized since July 2009 during the post-eruption phase (Grapenthin et al., 2013).

In the precursory phase before explosive eruption, gas was emitted and the glacier on the summit was melted (Buurman et al, 2013; Ketner and Power, 2013). Precursory seismic activity increased starting in November 2008 (Buurman et al, 2013). The first seismic swarm was composed of 897 events, and lasted for 31 hours since 26 February 2009. Four seismic swarms with ∼4500 events occurred before the explosive eruptions. The seismic swarms were caused by stress instability due to the upwelling of magma and increase in overpressurized gas. The mid-crustal magma accumulation at a depth of 3-9 km is indicated as the source of event-triggering between 1989 and 2010 (Power et al., 2013). The high seismicity and subsurface temperature caused the collapse of holes in the glacier.

The volcano erupted first in 22 March 2009 (Schaefer, 2012; Bull and Buurman, 2013). The exploisve eruptions occurred more than 20 times over 14 days (Bull et al., 2013; Schaefer,

2013). The last explosive eruption was observed on 4 April (Bull et al., 2013). After the explosive eruptions, lava domes grew slowly with lava flows (Buurman et al., 2013). The crater was deflated, accompanying continuous gas emission and decreases in pore pressure and temperature. The crack density in the medium increased. Pyroclastic flows swept the glacier valley and reached the Cook Inlet. Growth of the lava domes lasted until mid June. Seismic swarms with 7470 earthquakes occurred for 123 hours (Bull et al., 2013; Buurman et al., 2013). The seismic swarms were caused by stress instability induced by rockslides and gravitational collapse during lava dome growth (Buurman et al., 2013).

Procedure

The V_P/V_S ratios in the upper crust beneath the volcano are estimated by period using a modified Wadati analysis, enabling us to investigate the temporal variation of medium properties. The P and S velocity ratio, V_P/V_S, is determined by (Wadati, 1933; Jo and Hong, 2013):

$$\frac{V_P}{V_S} - 1 = \frac{(Ts - Tp)}{Tp}, \tag{1}$$

where T_P and T_S are the traveltimes of P and S waves.

The V_P/V_S ratios are estimated from P and S traveltimes using a linear regression based on equation (1). P and S traveltime data with deviations of 0.2 sec or greater from the least-squares line are removed from the analysis to improve the stability of the results (Fig. 1). The determination of the least-squares line and the removal of outliers are performed iteratively until no further data are removed. We analyze seismic data with epicentral distances equal to or less than 10 km, within which the medium is assumed to be homogeneous. The analysis is based on events with focal depths less than 10 km, which allows us to naturally constrain the depth of imaging.

The dense monitoring system and high seismicity enable stable estimation of V_P/V_S ratios in the study region, which is discretized by uniform cells with a size of 0.04° in longitude and 0.02° in latitude. Each cell overlaps with neighboring cells by 0.03° in longitude and 0.015° in latitude. The centers of the cells are placed every 0.01° in longitude and 0.005° in latitude.

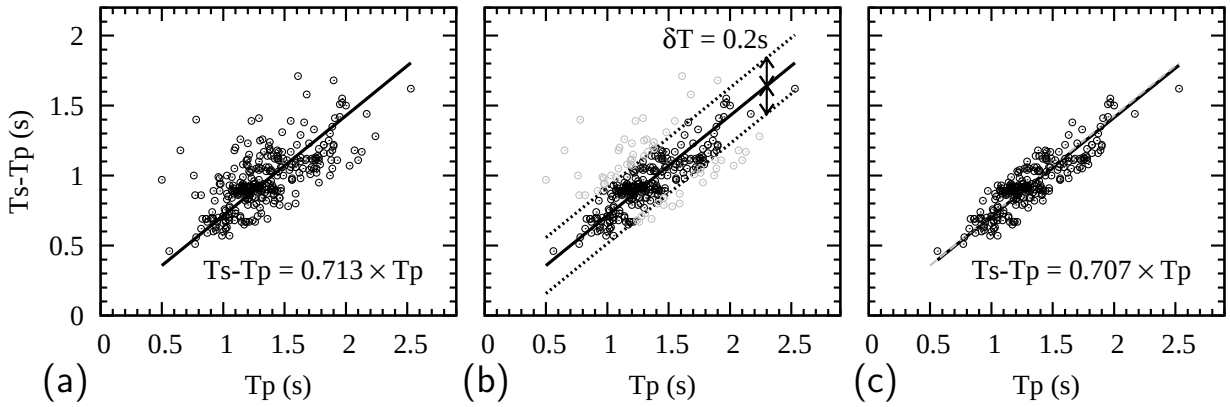

Figure 1. A schematic procedure of V_P/V_S measurement using a modified Wadati analysis: (a) determination of $V_P/V_S - 1$ from the original dataset using a linear regression, (b) removal of outliers with deviations greater than 0.2 sec from the least-squares line, and (c) redetermination of $V_P/V_S - 1$ from the selected dataset. The fitted line for the original dataset is presented in (c) with a gray dotted line for comparison. The refinement of $V_P/V_S - 1$ is repeated until no further data are removed.

The P and S traveltime dataset is classified by cell depending on the central locations of event-station pairs. A representative V_P/V_S ratio is estimated for every cell with more than 40 traveltime data using the modified Wadati method (Jo and Hong, 2013). The collection of V_P/V_S ratios for all cells represents the spatial variation of V_P/V_S ratios.

Fig. 2 presents the numbers of traveltime data over the cells. Regions around the volcano summit present a good data coverage with more than 300 traveltime data during periods I, II, and III. The numbers of traveltime data are 50 to 100 in most regions during periods IV and V.

The V_P/V_S ratio can be written in terms of the effective elastic moduli that are dependent on the porosity and composition of the pore fluids:

$$\frac{V_P}{V_S} = \sqrt{\frac{K_e}{\mu_e} + \frac{4}{3}}, \tag{2}$$

where K_e is the effective bulk modulus, and μ_e is the effective shear modulus. The effective bulk and shear moduli satisfy (Gassmann, 1951; Husen et al., 2004)

$$\frac{K_e}{K_r - K_e} = \frac{K_d}{K_r - K_d} + \frac{K_f}{\phi(K_r - K_f)}, \quad \mu_e = \mu_d, \tag{3}$$

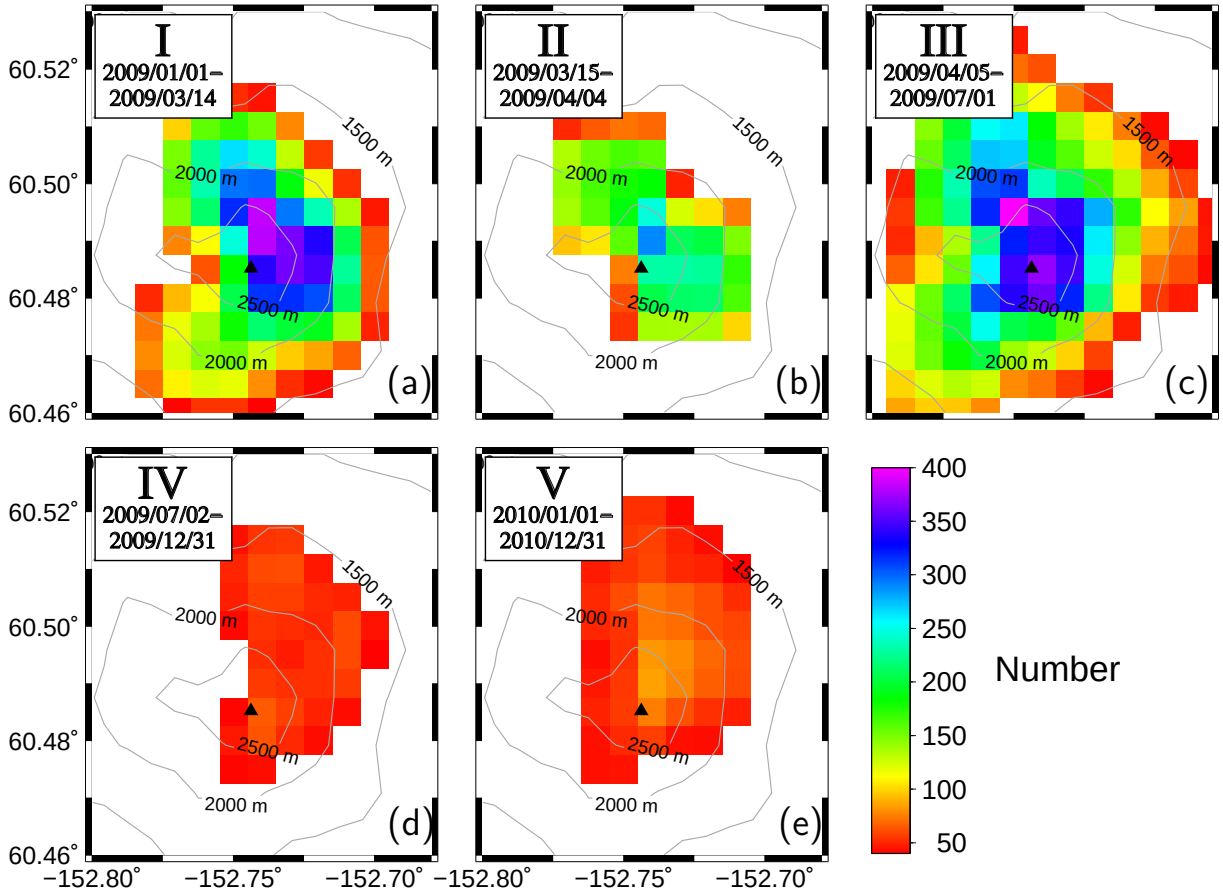

Figure 2. Numbers of data at discretized cells: periods (a) I, (b) II, (c) III, (d) IV, and (e) V. Contours for surface topography are drawn with gray lines. Only the cells with more than 40 traveltime data are presented. The numbers of data are large around the summit in periods I, II, and III.

where K_r is the bulk modulus of the rock matrix, K_d is the bulk modulus of dry rock with empty pores, K_f is the bulk modulus of the pore fluid, ϕ is the porosity of the rock, and μ_d is the shear modulus of dry rock with empty pores.

The elastic moduli of dry rock with empty pores can be written in terms of porosity ϕ (Nur et al., 1995; Husen et al., 2004):

$$K_d = K_r \left(1 - \frac{\phi}{\phi_c}\right), \quad \mu_d = \mu_r \left(1 - \frac{\phi}{\phi_c}\right), \tag{4}$$

where ϕ_c is the critical porosity that is set as 0.15 (Miller et al., 1998). The pore fluid is a mixture of liquids and gas. When the vertical variations in pressure (P) and temperature (T) are known, the elastic moduli of the rock matrix (K_r, μ_r) at a given depth can be calculated

from those on the Earth's surface and the increase rates of elastic moduli with pressure and temperature (dK/dP, dK/dT, $d\mu/dP$, and $d\mu/dT$). The elastic moduli at a certain depth can be calculated by

$$K_r = K_0 + \frac{dK}{dP}\Delta P + \frac{dK}{dT}\Delta T,$$
$$\mu_r = \mu_0 + \frac{d\mu}{dP}\Delta P + \frac{d\mu}{dT}\Delta T, \tag{5}$$

where K_0 and μ_0 are the elastic moduli on the Earth's surface, ΔP is the differential pressure, and ΔT is the differential temperature.

The elastic moduli of the rock matrix (K_r, μ_r) are dependent on the chemical composition, temperature, and pressure. The elastic moduli (K_r, K_d, K_f, μ_r, and μ_d) for a certain rock matrix and fluid composition at a given depth can be calculated, which allows us to determine the V_P/V_S ratio from equation (2). Thus, the V_P/V_S ratio is dependent on the fluid composition and properties of the medium. The temporal changes in V_P/V_S ratios provide information on the variation of fluid properties.

The prevailing rock in the medium is andesite that is composed of 60 % SiO_2, 20 % Al_2O_3, 10% CaO, and 10% MgO. The elastic moduli at normal temperature and pressure (298°K, 1 bar) and the derivatives of elastic moduli for pressure and temperature (dK/dP, dK/dT, $d\mu/dP$, and $d\mu/dT$) are collected (Anderson et al., 1968). The representative depth of medium is considered to be 5 km, at which the temperature is approximately 225°C and the lithostatic pressure is 0.13 GPa (Wyndman, 1985).

Stability test

The V_P/V_S ratio is dependent on the traveltimes of P and S waves (T_P, T_S). Errors in traveltimes may cause incorrect estimation of the V_P/V_S ratio. The stability of V_P/V_S estimates is tested using a bootstrapping resampling analysis (Efron and Tibshirani, 1991). The bootstrap analysis randomly resamples data from the original full dataset with allowance of duplicate selection. The bootstrap analysis examines the stability of the dataset, and assesses plausible errors in the estimates (Hong and Menke, 2008; Jo and Hong, 2013).

One hundred resampled datasets are prepared, and the V_P/V_S ratios are estimated. The

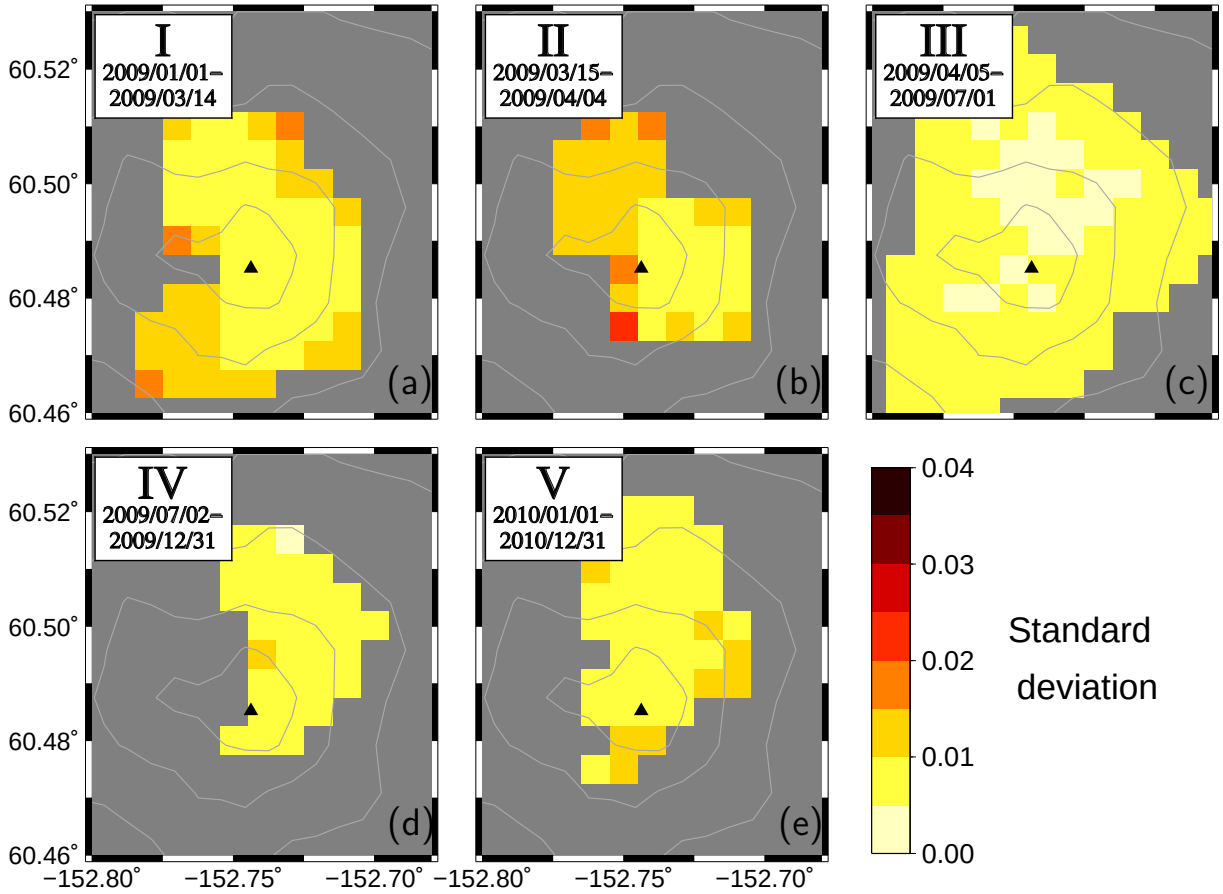

Figure 3. Standard deviations of V_P/V_S ratios among 100 resampled datasets based on bootstrapping method: periods (a) I, (b) II, (c) III, (d) IV, and (e) V. The standard deviations are less than 0.02 in most regions of all periods. The bootstrap analysis suggests the stability of results.

V_P/V_S estimates are found to be similar among the 100 resampled datasets. The standard deviations among the V_P/V_S ratios of the 100 resampled datasets are less than 0.016, with an average of 0.010±0.003 for period I, 0.020 with an average of 0.011±0.003 for period II, 0.010 with an average of 0.006±0.001 for period III, 0.010 with an average of 0.008±0.001 for period IV, and 0.011 with an average of 0.009±0.001 for period V. The standard deviations are small enough to be negligible considering plausible errors associated with the traveltime data. It is also observed that the all the V_P/V_S estimates from the 100 resampled datasets are similar to those based on the original dataset (Fig. 3). The observation suggests that the results are stable and rarely dependent on the datasets.

We assess the influence of plausible errors in the phase arrival times on V_P/V_S estimates.

Local P and S waveforms are impulsive, enabling us to identify the arrival times of P and S waves with high precision. S waves typically have larger picking errors than P waves due to their relatively low frequency contents and contamination by P coda. Considering the epicentral distances, focal depths, and sampling rates of records, phase picking errors of P and S may not exceed 0.05 and 0.1 sec, respectively. White random errors between -0.05 and 0.05 sec are applied to the original P traveltimes, and those between -0.1 and 0.1 sec are applied to the original S traveltimes. The V_P/V_S ratios are then estimated for the error-added traveltime dataset. The errors in V_P/V_S ratios, $|\Delta(V_P/V_S)|$, are found to be less than 0.027 with an average of 0.006±0.005 for period I, 0.023 with an average of 0.008±0.006 for period II, 0.014 with an average of 0.004±0.003 for period III, 0.021 with an average of 0.006±0.005 for period IV, and 0.019 with an average of 0.006±0.005 for period V (Fig. 4). The V_P/V_S errors induced by the traveltime errors are less than 0.015 in most regions during all periods. This observation suggests that traveltime errors do not produce large errors in the analysis.

We also examine the potential influence of origin time errors on the V_P/V_S estimates. Errors in origin times naturally incorporate errors in hypocentral locations. White random noises between -0.2 and 0.2 sec are applied to the origin times. The errors in origin times are equivalent to hypocentral-location errors equal to or less than ∼1.5 km, considering the seismic velocities in the crust. The origin time errors introduce the same sizes of errors to both P and S traveltimes. The errors in V_P/V_S ratios, $|\Delta(V_P/V_S)|$, are observed to be less than 0.040 with an average of 0.011±0.009 for period I, 0.033 with an average of 0.014±0.009 for period II, 0.020 with an average of 0.006±0.004 for period III, 0.018 with an average of 0.007±0.005 for period IV, and 0.027 with an average of 0.008±0.006 for period V (Fig. 5). It is observed that the V_P/V_S errors induced by the origin-time errors are less than 0.02 in most regions during all periods. The origin-time errors introduce slightly larger errors in V_P/V_S ratios than the arrival-time errors. However, the V_P/V_S errors are found to be small enough to support the stability of the results.

We finally combine the arrival-time errors and origin-time errors together, and assess the errors in V_P/V_S ratios. The P arrival-time errors between -0.05 and 0.05 sec, S arrival-time errors between -0.1 and 0.1 sec, and origin time errors between -0.2 and 0.2 sec are added to the original traveltime dataset. The errors in V_P/V_S ratios, $|\Delta(V_P/V_S)|$, are less than 0.040

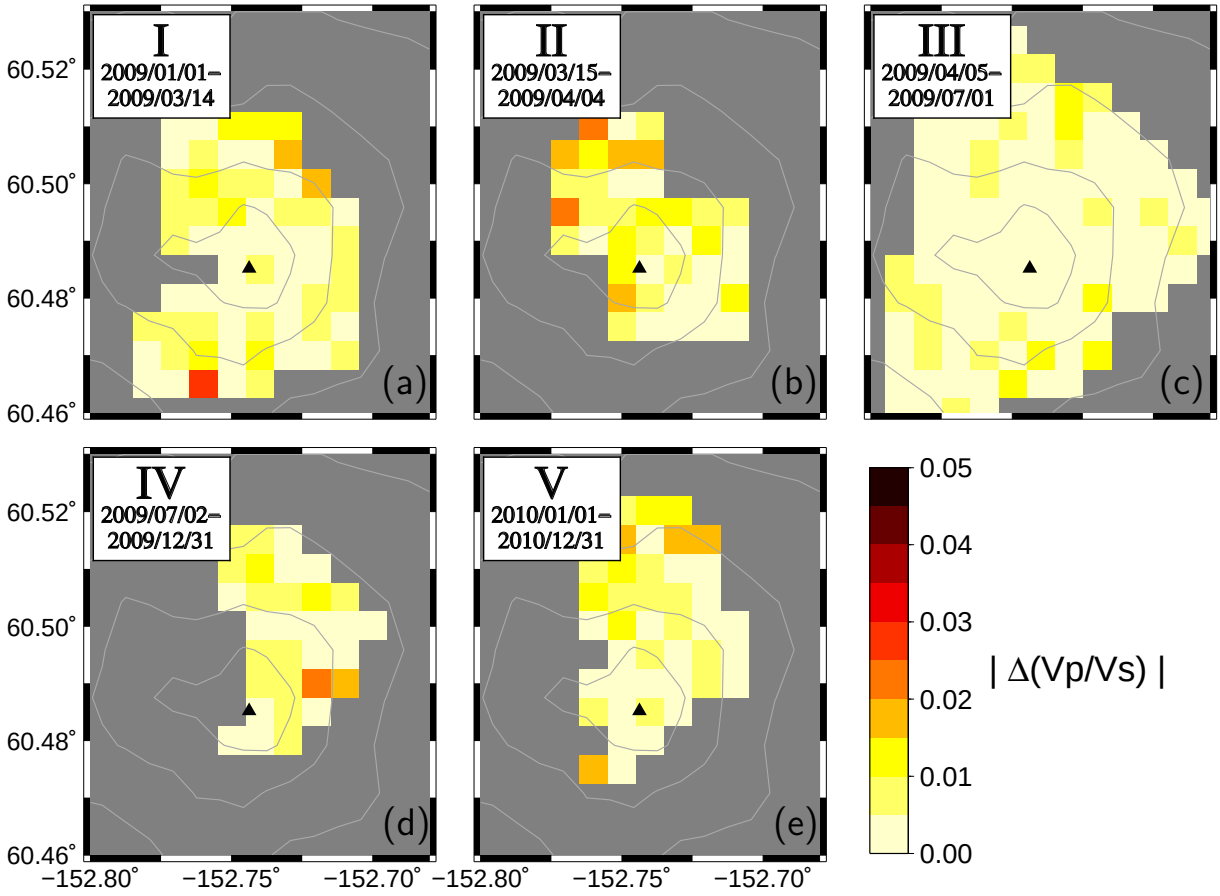

Figure 4. Errors in V_P/V_S ratios induced by plausible traveltime errors: periods (a) I, (b) II, (c) III, (d) IV, and (e) V. White random errors between -0.05 and 0.05 sec are applied to P traveltimes, and those between -0.1 and 0.1 sec to S traveltimes. The errors in V_P/V_S ratios are found to be less than 0.015 in most regions of all periods, suggesting the validity of the V_P/V_S estimates.

with an average of 0.012±0.009 for period I, 0.036 with an average of 0.013±0.009 for period II, 0.026 with an average of 0.007±0.005 for period III, 0.021 with an average of 0.007±0.005 for period IV, and 0.027 with an average of 0.011±0.007 for period V (Fig. 6). The V_P/V_S errors are increased slightly for the implementation of combined errors compared to those for the implementation of either arrival-time errors or origin-time errors. The V_P/V_S errors are, however, still less than 0.02 in most regions for all periods. The stability tests suggest that the results are stable and reliable for possible contamination by errors in datasets.

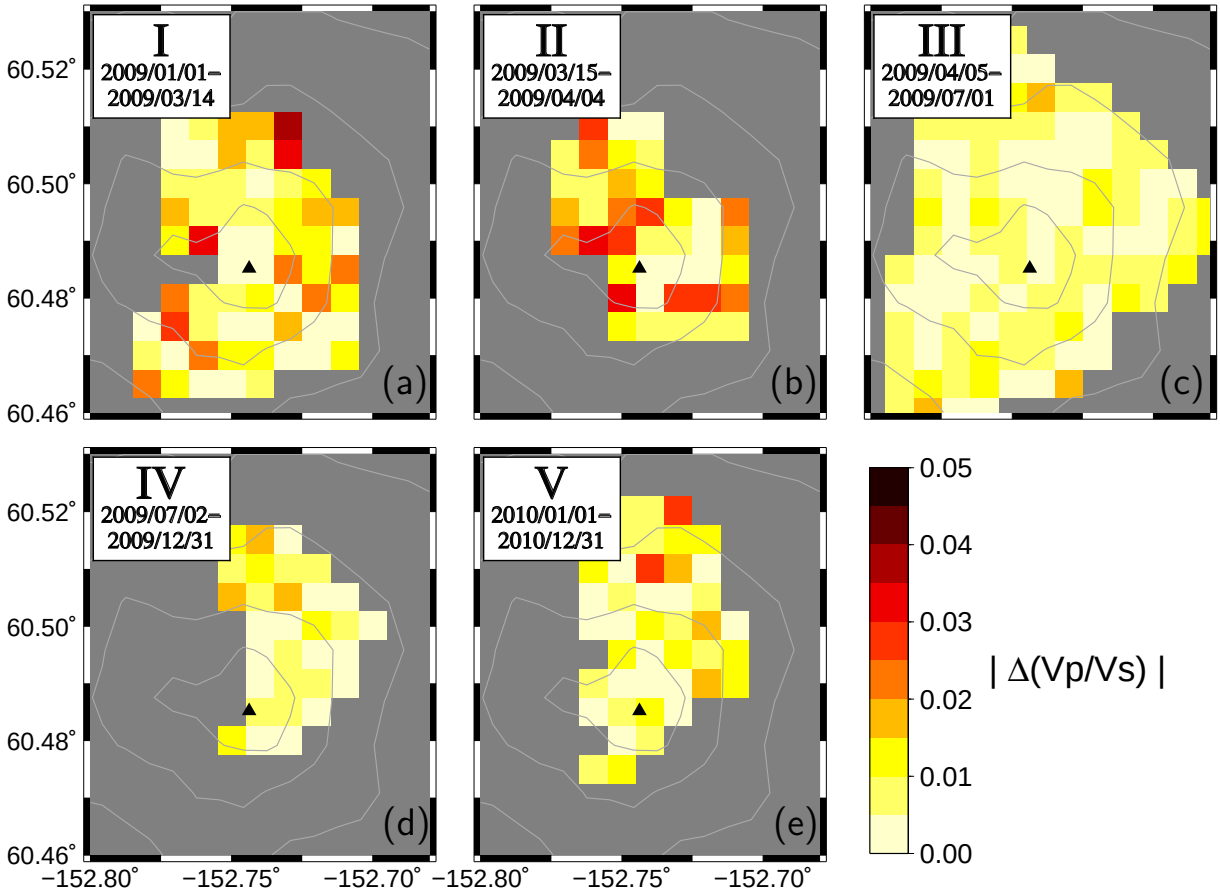

Figure 5. Errors in V_P/V_S ratios induced by plausible errors in origin times: periods (a) I, (b) II, (c) III, (d) IV, and (e) V. White random errors between -0.2 and 0.2 sec are applied to the origin times. The errors in V_P/V_S ratios are found to be less than 0.02 in most regions of all periods, suggesting the validity of the V_P/V_S estimates.

Poisson's ratios

The estimated V_P/V_S ratios can be converted to Poisson's ratios, σ by:

$$\sigma = \frac{1}{2}\left[1 - \frac{1}{(V_P/V_S)^2 - 1}\right]. \tag{6}$$

The Poisson's ratios of period I are determined to be 0.27-0.33 with an average of 0.31 and standard deviation of 0.013, those of period II to be 0.29-0.34 with an average of 0.31 and standard deviation of 0.015, those of period III to be 0.23-0.29 with an average of 0.25 and standard deviation of 0.011, those of period IV to be 0.24-0.26 with an average of 0.25 and

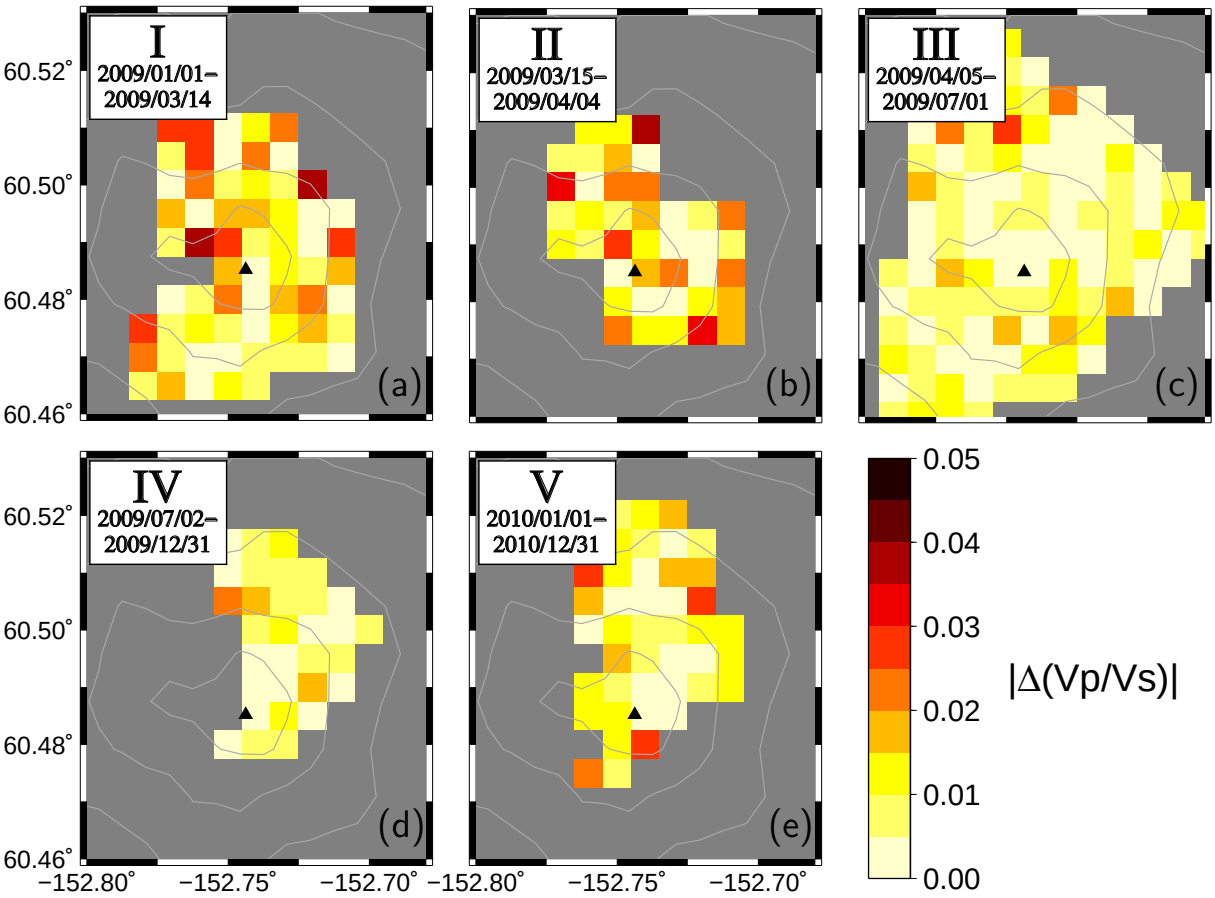

Figure 6. Errors in V_P/V_S ratios induced by combined errors in arrival times and origin times: periods (a) I, (b) II, (c) III, (d) IV, and (e) V. The errors in V_P/V_S ratios are less than 0.02 in most regions for all periods.

standard deviation of 0.006, and those of period V to be 0.23-0.26 with an average of 0.25 and standard deviation of 0.008 (Fig. 7).

References

Andeson, O.L., E. Schreiber, R.C. Liebermann (1968). Some elastic constant data on minerals relevant to geophysics, Reviews of Geophysics, 6 491-524.

Bleick, H.A., M.L. Coombs, P.F. Cervelli, K.F. Bull, and R.L. Wessels (2013). Volcano-ice interactions

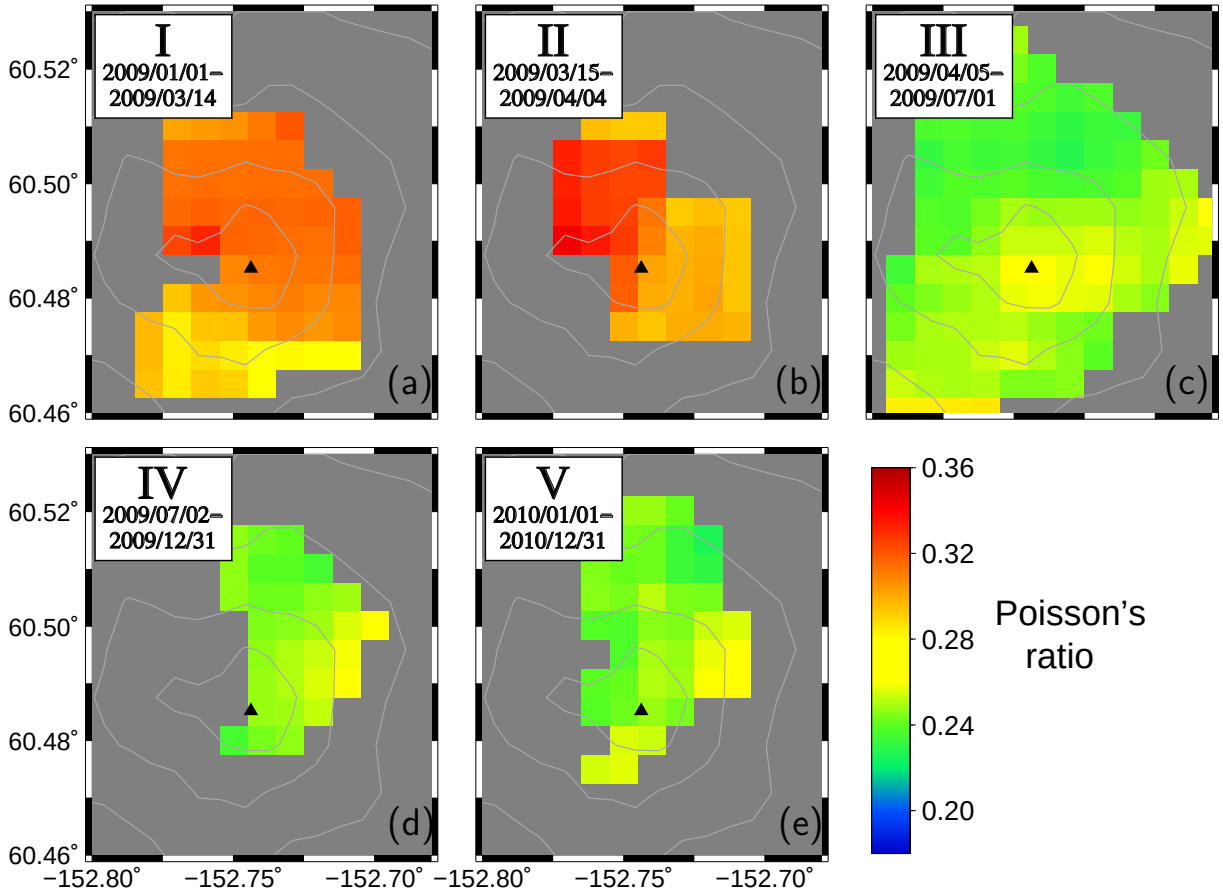

Figure 7. Poisson's ratios equivalent to the V_P/V_S ratios: periods (a) I, (b) II, (c) III, (d) IV, and (e) V. High Poisson's ratios of 0.31 on average are observed in periods I and II, and low Poisson's ratios of 0.25 on average are found in periods III, IV, and V.

precursory to the 2009 eruption of Redoubt Volcano, Alaska, Journal of Volcanology and Geothermal Research, 259, 373-388.

Bull, K.F., S.W. Anderson, A.K. Diefenbach, R.L. Wessels, and S.M. Henton (2013). Emplacement of the final lava dome of the 2009 eruption of Redoubt Volcano, Alaska, Journal of Volcanology and Geothermal Research, 259, 334-348.

Bull, K.F., and H. Buurman (2013). An overview of the 2009 eruption for Redoubt Volcano, Alaska, Journal of Volcanology and Geothermal Research, 259, 2-15.

Buurman, H., M.E. West, and G. Thompson (2013). The seismicity of the 2009 Redoubt eruption, Journal of Volcanology and Geothermal Research, 259, 16-30.

Coombs, M., T. Sisson, H. Bleick, S. Henton, C. Nye, A. Payne, C. Cameron, J. Larsen, K. Wallace, and

K.F. Bull (2013). Andesites of the 2009 eruption of Redoubt Volcano, Alaska, Journal of Volcanology and Geothermal Research, 259, 349-372.

Efron, B., and R. Tibshirani (1991). Statistical data analysis in the computer age, Science, 253, 390-395.

Husen, S., R.B. Smith, and G.P. Waite (2004). Evidence for gas and magamtic sources beneath the Yellowstone volcanic field from seismic tomographic imaging. Journal of Volcanology and Geothermal Research, 131, 397-410.

Gassmann, F. (1951). Uber die Elastizitat poroser Medien, Veirteljahrsschrift der Naturforschenden Gesellschaft in Zurich, 96, 1-23.

Grapenthin, R., J.T. Freymueller, and A.M. Kaufman (2013). Geodetic observations during the 2009 eruption of Redoubt Volcano, Alaska, Journal of Volcanology and Geothermal Research, 259, 115-132.

Hong, T.-K., and W. Menke (2008). Imaging laterally varying regional heterogeneities from seismic coda using a source-array analysis, Physics of the Earth and Planetary Interiors, 166, 188-202.

Jo, E., and T.-K. Hong (2013). V_P/V_S ratios in the upper crust of the southern Korean Peninsula and their correlations with seismic and geophysical properties, Journal of Asian Earth Sciences, 66, 204-214.

Ketner, D., and J. Power (2013). Characterization of seismic events during the 2009 eruption of Redoubt Volcano, Alaska, Journal of Volcanology and Geothermal Research, 259, 45-62.

Miller, A.D., B.R. Julian, and G.R. Foulger (1998). Three-dimensional seismic structure and moment tensors of non-doublecouple earthquakes at the Hengill-Grensdalur volcanic complex, Iceland, Geophysical Journal International, 133, 309-325.

Morrissey, M.M. (1997). Long-period seismicity at Redoubt Volcano, Alaska, 1989-1990 related to magma degassing, Journal of Volcanology and Geothermal Research, 75, 321-335

Nur, A., G. Mavko, J. Dvorkin, and D. Gal (1995). Critical porosity: The key to relating physical properties to porosity in rocks, proceedings of the 65th Annual International Meeting, Society of Exploration Geophysicists, 878 pp.

Power J.A., S.D. Stihler, B.A. Chouet, M.M. Haney, and D.M. Ketner (2013). Seismic observations of Redoubt Volcano, Alaska- 1989-2010 and a conceptual model of the Redoubt magmatic system, Journal of Volcanology and Geothermal Research, 259, 31-44.

Schaefer, J.R. (2012). The eruption of Redoubt Volcano, Alaska. Alaska Division of Geological and Geophysical Surveys Report of Investigations 2011-5, 45 pp.

Schaefer, J.R., C.E. Cameron, and C.J. Nye (2009). Historically active volcanoes of Alaska: Alaska

Division of Geological and Geophysical Surveys Miscellaneous Publication 133, 1 sheet, scale 1:3,000,000.

Wadati, K., (1933). On the travel time of earthquake waves, II, Geophysical Magazine, 7, 101-111.

Wyndman, D.W. (1985). Petrology of igneous and metamorphic rocks, 2nd ed., McHraw- Hill Book Company.